The Seismic Record
A journal of the Seismological Society of America

Reverse-Polarity Earthquakes at Intermediate Depth in North Chile and Bolivia: Observations of a Rare Phenomenon

OPEN ACCESS

Jonas Folesky*[1], Jörn Kummerow[1], Gesa Petersen[2], and Laurens Jan Hoffman[1,3]

Abstract

To date, there are only a few well-documented examples of reverse-polarity earthquakes worldwide, especially at intermediate depth. These are pairs or families of very closely located events, where one or more members show flipped polarities, indicating nearly reversed earthquake mechanisms. We identify four intermediate-depth reverse-polarity earthquake families in a catalog of originally 3153 repeating earthquake sequences for the North Chilean subduction zone from 2006 to 2024. A detailed analysis of the largest group, which consists of 38 events and contains five reverse events, is presented. Relative event relocations, cluster properties, and interevent times suggest a very small active volume of the order of only a few hundred meters, partially with overlap of the rupture area, and a weak upward migration of seismicity over several years. As uncertainties remain, we discuss several possible models to explain the observations. We propose that they may reflect transient processes linked to dehydration embrittlement and fluid pulses.

Cite this article as Folesky, J., J. Kummerow, G. Petersen, and L. Jan Hoffman (2026). Reverse-Polarity Earthquakes at Intermediate Depth in North Chile and Bolivia: Observations of a Rare Phenomenon, *The Seismic Record*. **6**(**3**), 329–337, doi: 10.1785/0320260015.

Supplemental Material

Introduction

Repeating earthquakes are an expression of reiterative activation of the same fault patch, with a complete or at least significant overlap of the rupture area. They can be used to characterize the local slip behavior, dynamics, and fine structure of faults at depths that are inaccessible to other methods (Nadeau and McEvilly, 1999; Igarashi *et al.*, 2003). Repeating earthquakes occur in creeping environments, often at the transition between seismic and aseismic zones, and have been found in many regions on Earth. They are commonly identified by cross-correlation of the seismological waveform data as a measure of event similarity. We refer to Uchida and Bürgmann (2019) for a more detailed overview.

In this study, we use the same approach that is often used for detecting regular repeating earthquakes to identify reverse-polarity earthquakes; that is, we compute the normalized cross-correlation coefficient (cc) to search for earthquakes with highly similar waveforms but reverse-polarity (that is, negative correlations close to cc = −1.0). Figure 1 shows an illustrative waveform example from North Chile. In contrast to normal repeating earthquakes, which have positive correlations close to cc = + 1.0, reports of such highly anticorrelated event combinations are extremely rare. They imply colocation, but reversed mechanisms, and since earthquakes generally reflect the local stress field and fault orientation, similar or identical mechanisms are to be expected if their locations coincide and conditions are stable in time.

As of today, only a few observations of reverse-polarity earthquakes have been reported. Prieto *et al.* (2012) identified examples of reverse-polarity waveforms from multiple stations for several events in the Bucaramanga earthquake nest at about 160 km depth in Colombia. Ma and Wu (2013) found five

1. Department of Geophysics, Freie Universität Berlin, Berlin, Germany, https://orcid.org/0000-0002-7729-9624 (JF); https://orcid.org/0000-0002-6026-5911 (JK); https://orcid.org/0000-0002-1791-8489 (LJH); 2. GFZ Helmholtz Centre for Geosciences, Potsdam, Germany, https://orcid.org/0000-0002-7138-0499 (GP); 3. Now at InterWorks, Berlin, Germany

*Corresponding author: jonas.folesky@geophysik.fu-berlin.de

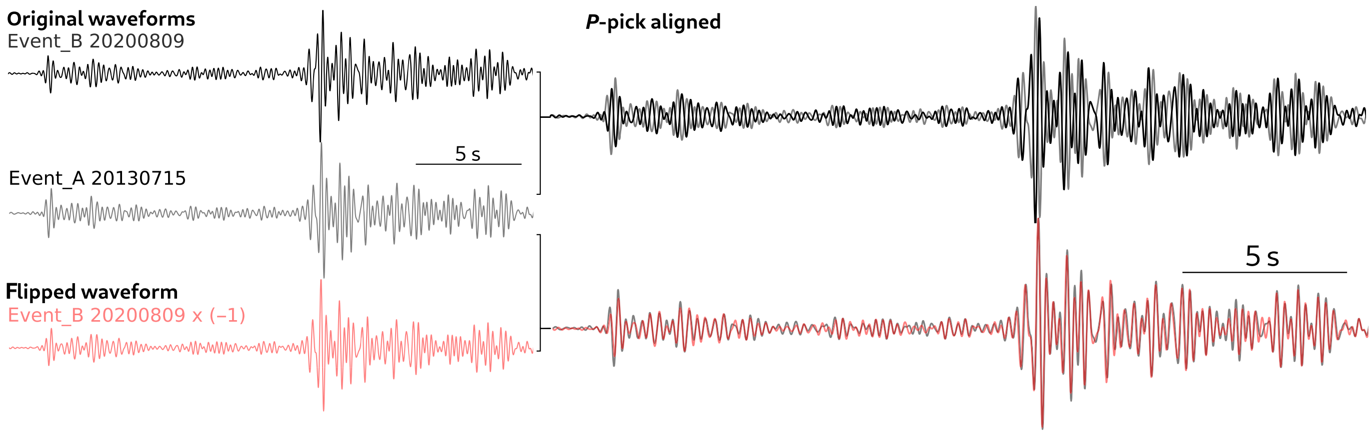

Figure 1. Normalized waveforms of a reverse-polarity pair (cID 1982 in Folesky *et al.*, 2025) recorded at the Integrated Plate Boundary Observatory Chile, IPOC(CX) station PB01. The band-pass filter is 1–5 Hz. Event A occurred in 2013 and event B in 2020. On the left, the original waveforms are displayed in black and gray. The red waveform is the amplitude-flipped waveform of event B. On the right, the aligned waveforms are shown. The black and gray are the original traces, and the red is the flipped waveform. Note the very high similarity between the seismogram of event A and the flipped wavetrain of event B. More waveform examples are shown in the supplement.

doublets among 2631 aftershocks of the 2008 Wenchuan, China, earthquake, with flipped polarity observed on all three components of a nearby station. Trugman *et al.* (2020) detected 45 pairs of anti-similar earthquakes with cc < −0.85 among 30,000 aftershocks of the 2019 Ridgecrest, California, mainshocks, with interevent separations of hundreds of meters. Also in Ridgecrest, Shearer *et al.* (2024) conducted a very detailed study of one reverse-polarity pair. From the analysis of subtle variations of the *S* to *P* amplitude and waveform-based relocation, they concluded that the events were separated by about a hundred meters, occurred on fault planes with slightly different orientations, and were probably caused by local stress heterogeneity. A similar observation was made by Lu *et al.* (2025) in Nevada, United States.

Recently, Cesca *et al.* (2024) provided an overview of more reported observations of so-called anti-repeaters in various environments from laboratory to field scales and discussed different physical processes to explain them. They separated cases of reverse-polarity events into true anti-repeaters, which activate the same fault patch, and quasi anti-repeaters, which occur at only neighboring locations without source overlap. Importantly, they noted that in most previously reported cases, location uncertainties do not allow distinguishing between the two categories. A follow-up systematic study provided a first global catalog for this specific subset of seismological events (Cesca *et al.*, 2026).

In this work, we use a regional repeater catalog for the northern Chilean subduction zone (Folesky *et al.*, 2025) to identify and characterize reverse-polarity earthquakes, to improve our understanding of their physical mechanisms. We present our identification criteria, relocate the events, examine their partial source overlap, and discuss the temporal event evolution—findings that collectively support event colocation. Finally, we discuss potential physical models to explain reverse-polarity events at intermediate depths and compare our observations with the very limited existing literature on similar events.

Seismicity Data

This study is based on continuous seismological waveform data from North Chile, recorded by the Integrated Plate boundary Observatory Chile (IPOC) (2006) station network (Fig. 2). We use the recent repeating earthquake catalog from Folesky *et al.* (2025) that covers a time period of nearly two decades from late 2006 to 2024 to explicitly search for reverse-polarity events. For detailed information on data availability, we refer to figure S1 in Folesky *et al.* (2025). The authors computed pairwise CCs at the three to five closest stations for time windows of distance-dependent length, which always included both *P* and *S* phases. Negative cc values for which absolute values exceeded positive cc values of the next cycle (compare with Cesca *et al.*, 2024) were explicitly taken into account. The utilized vertical-component broadband displacement data were band-pass filtered between 1 and 4 Hz. Note that the application of such long time windows prevents identifying event pairs that only have a highly anti-similar *P* phase or an *S* phase, as reported for several examples in Shearer *et al.* (2024).

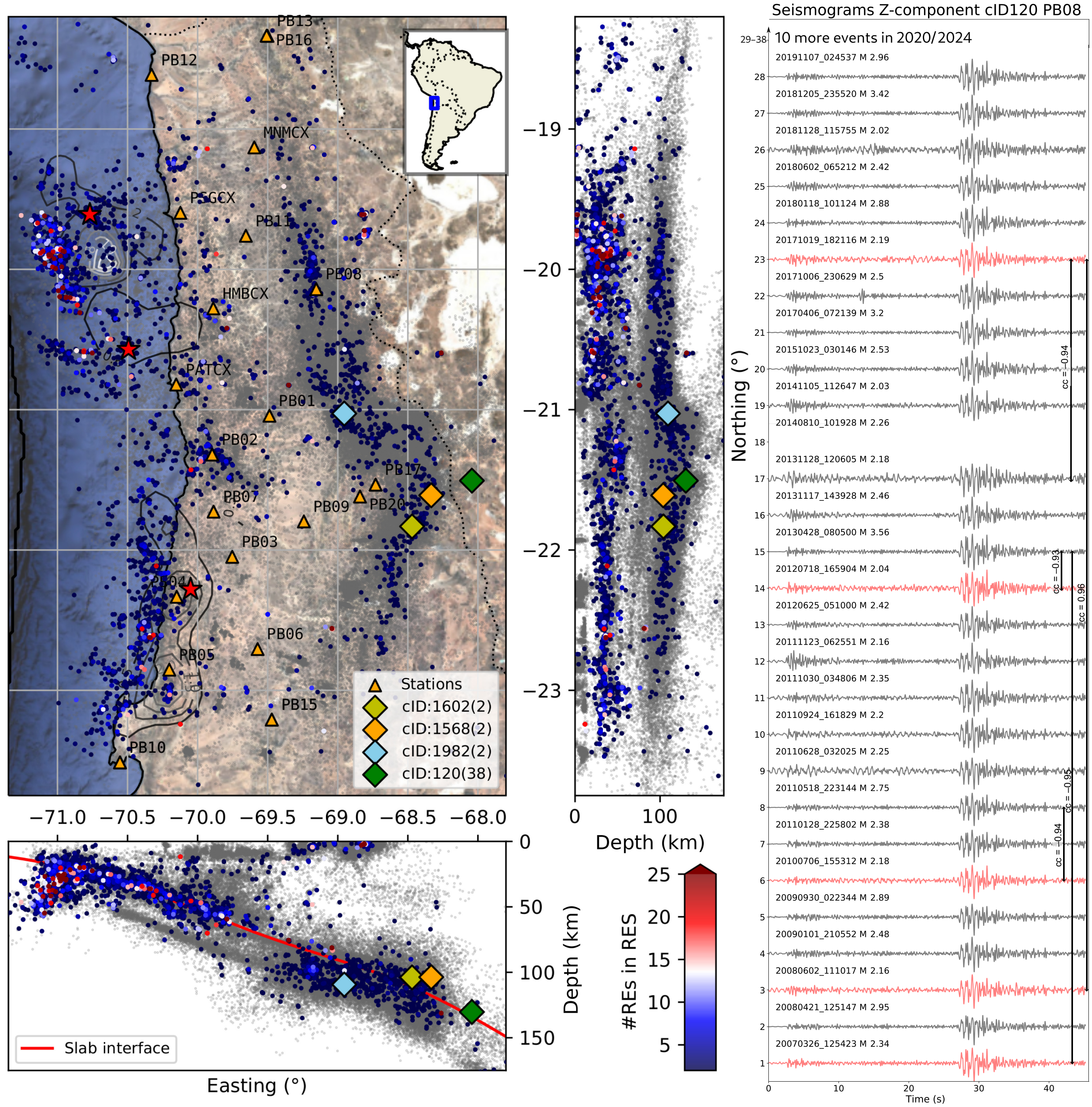

Figure 2. Four reverse-polarity families in North Chile and Bolivia (colored diamonds), plotted on top of repeating earthquake family locations in the target region, taken from the repeater catalog of Folesky *et al.* (2025). Here, blue to red colors indicate the number of repeaters in a given sequence. The diamond legend entries indicate the family cluster IDs and the total number of events in the sequences in brackets. The orange triangles are IPOC station locations. From north to south, red stars are the hypocenters of the 2014 M_w 8.1 Iquique earthquake, its M_w 7.7 aftershock, and the 2007 M_w 7.7 Tocopilla earthquake. For references to their slip contours, we refer the reader to Folesky *et al.* (2025). The gray background seismicity is from Sippl *et al.* (2023). On the right, vertical-component waveforms for group cID120 are shown (1–5 Hz, normalized), recorded at station PB08. For lack of space, only 28 out of 38 events are shown here. The red events are the reverse-polarity events, where waveforms are flipped for display here. Their highest cc match is indicated to the right. The horizontal components, additional waveforms recorded at other stations, and the full cc matrices are shown in the supplement.

We consider all pairs of events for which the negative cross-correlation value lies below cc ≤ −0.95 at a minimum two stations. The sequences that contain one or more anticorrelated event combinations are defined as reverse-polarity series, where the majority of events (or, in the case of doublets, the first occurrence) determine the regular sense, and the minority the inverse. An example of waveforms of an anticorrelated pair is shown in Figure 1. More seismogram data, including horizontal components and records from additional stations, are provided in the supplement, available to this article.

Data Analysis and Results

From the 3153 repeating earthquake sequences in Folesky *et al.* (2025), we find only four sequences that contain at least one reverse-polarity event. Their origin times, hypocenters, magnitudes, and estimated slips are listed in Table S1. Three groups are just event pairs, but the remaining group (cID120) consists of 38 events, of which five show reversed polarity (Fig. 2; see the supplement for waveforms at two more stations).

All four groups have median hypocenter depths greater than 100 km, and their magnitudes range mainly between $1.8 \le M \le 3.5$. The three doublets lie in or on top of the most intensive seismicity spots in the entire background catalog (Sippl *et al.*, 2023), whereas the group cID120 is located farther east, several kilometers outside the cloud. In general, these intermediate depths are atypical for normal repeating earthquakes, as the common model is the repeated activation of a fault patch loaded by adjacent creeping areas, which is usually observed at shallower depths and along the plate interface (Nadeau and McEvilly, 1999; Uchida and Bürgmann, 2019). This concept appears to be suitable for the seismicity located at the intact plate interface, that is, at shallower depths (about <50 km). Also in northern Chile, most of the observed repeating earthquake sequences concentrate at the shallow plate interface, and repeater sequences of more than five events are rare at depths larger than 80 km (compare with Fig. 2) even though roughly 80% of the cataloged seismicity occurs at intermediate depth (Sippl *et al.*, 2023).

In the following, we will focus our analysis on the exceptional multievent reverse-polarity sequence cID120. We will focus on establishing whether the reverse-polarity events are anti-repeaters, that is, have identical rupture planes with other events from that family, and to what extent they differ from the prograde sequence members.

According to the Integrated Plate boundary Observatory Chile (IPOC) catalog (Sippl *et al.*, 2023), this event group is located just east of the highly active intermediate-depth seismicity cloud, at a depth of 133 km (green diamond in Fig. 2). The uncertainty of the catalog locations for this series outside the geometry of the station network is substantial (≫5 km, Sippl *et al.*, 2023). It therefore remains uncertain whether the group is situated in the slab, on top of it, or in the mantle above. However, we reaffirm its isolated position by studying the waveform-based interconnection with neighboring earthquakes in the region (Igarashi *et al.*, 2003). The resulting cc value histogram shows a distinct bimodal distribution, clearly separating the events within the sequence from the remaining earthquakes (compare with Figs. S9 and S10). We interpret this as a physical separation of the group from the intermediate-depth cloud.

We resolve in more detail the internal structure of the sequence by combining information from precise event relocation, agglomerative clustering, and spatiotemporal event analysis. In particular, this is intended to clarify if the reverse-polarity events form a distinct subgroup within the sequence.

First, we perform relative event relocation, using relative $S-P$ travel-time differences which are refined by waveform cross-correlation. These times are inverted based on the absolute locations and the source–receiver ray paths provided by the NonLinLoc location program (Lomax *et al.*, 2000). The method notably uses only stations with differential P and differential S times for the pairs of events. We refer the reader to the supplement for a detailed description of our method. The relative event location effectively collapses the cloud to a volume with a spatial extent of only a few hundred meters (Fig. 3a, b), compared with a spread of several tens of kilometers in the original catalog (Fig. S9). We derive formal errors for the relocated hypocenters by assuming standard errors of ±10 ms for the measured cross-correlation-based differential times for which we computed 500 noise-perturbed location iterations. The resulting location errors inferred from the 1σ standard deviations are about 60 m in vertical and 20–30 m in horizontal directions.

Second, we apply agglomerative clustering to separate the group into subclusters. We average the absolute values of the best three cc values for each pair of events at all available stations (where the pairs of events have data and phase picks). Together, these values build a connectivity matrix that is fed into the scikit-learn agglomerative clustering algorithm (Buitinck *et al.*, 2013) using the Ward method, which minimizes the distance (here cc value) variance of the merged clusters. This results in groupings of events that have slightly higher similarity among each other than with events in the

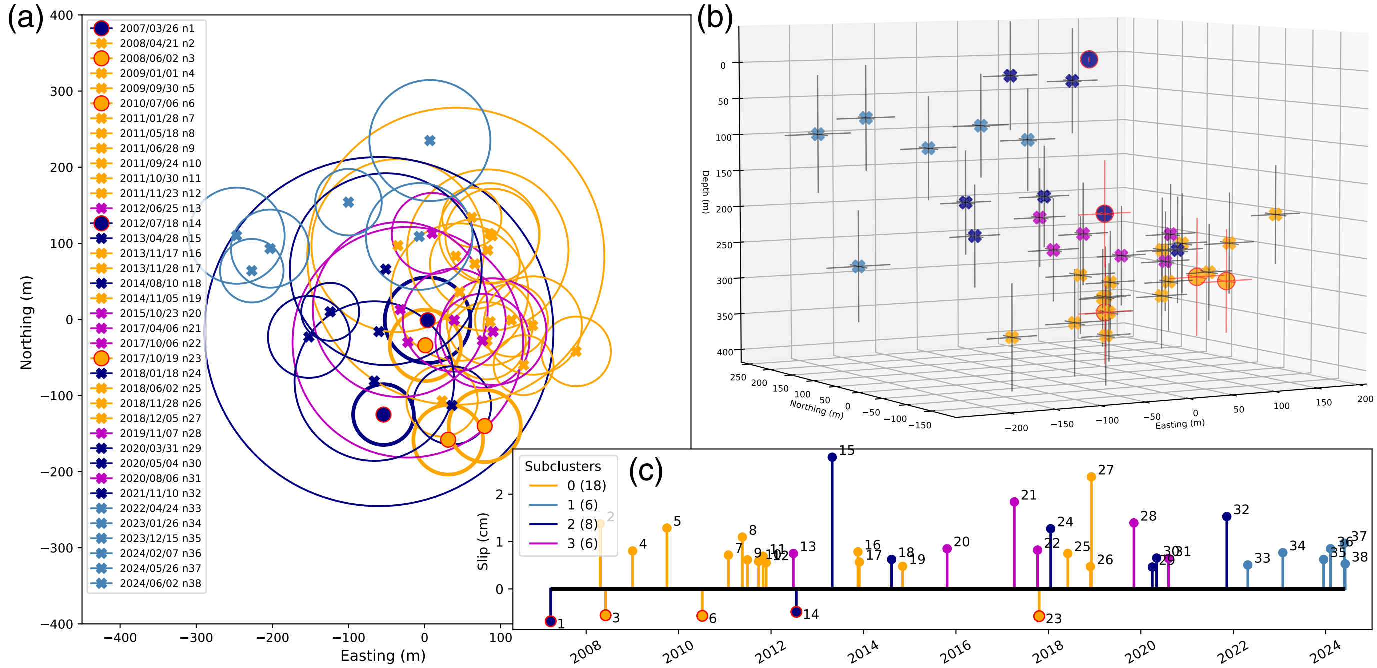

other subgroups. Representations of the matrix are shown in Figures S11 and S12. The waveform similarity-based classification into subclusters and the relocated hypocenters, computed independently from differential travel times, show a consistent pattern (Fig. 3a,b, where the color coding corresponds to the clustering). For a preselected number of four groups, we obtain an eastern group (orange, $n = 18$), a northwestern group (light blue, $n = 6$), a central group (blue, $n = 8$), and a central–eastern group (magenta, $n = 6$). Interestingly, the reverse-polarity events do not form a separate subcluster but split into the central and eastern groups. Note that we use, of course, absolute cc values for computing the subclusters. In other words, the reverse-polarity events are more strongly anticorrelated with some prograde events in the series than they are correlated with other reverse-polarity events. The 3D plot also reveals a tendency in the relocated hypocenters to migrate upward over time.

Third, we compute the source dimensions for all events in the series. For this, we assume a fixed stress-drop value of 10 MPa, plausible for the given depth range in northern Chile (Folesky, 2024; Folesky *et al.*, 2024) and similarly used in comparable studies at other locations and depths (e.g., Nakajima *et al.*, 2013). Using the seismic moment M_0 obtained from the given catalog magnitudes (Sippl *et al.*, 2023), and applying the Hanks and Kanamori (1979) relation and Eshelby (1957) circular fault model, we obtain estimates of the rupture radius as

Figure 3. (a,b) Relocated events of family cID120, with location errors plotted in (b). The five reverse-polarity events are indicated by a central filled dot. The color corresponds to subclusters. The circle sizes are computed individually from the event magnitudes and stress drops according to equation (1). Note the consistency of location with subcluster colors, even though clustering was performed independently of location, based solely on cc connectivity. Also note that the reverse-polarity events belong to two different subclusters rather than forming a separate cluster. A version with event occurrence history-based coloring is available in Figure S13. (c) Slip history of cID120. Reverse-polarity events are indicated by negative slip values highlighted by red outlines. The vertical lines are colored by association to the subclusters in panel (a). Note that in three out of five cases (events 3, 14, and 23) the reverse event is preceded by a regular event with only a very short waiting time between both.

$$\Delta\sigma = \frac{7\pi\mu\overline{D}}{16r} = \frac{7M_0}{16r^3} <=> r = \left(\frac{7M_0}{16\Delta\sigma}\right)^{\frac{1}{3}}, \quad (1)$$

in which $\overline{D}$ is the average slip over the fault, and μ is the rigidity. The radii of the ruptures vary between $40 \leq r \leq 230$ m, whereas the spread of the magnitudes in that group ranges between $2.0 \leq M \leq 3.5$ (compare with Table S1, see also Fig. 3a).

The diameter of the activated volume after relocation is approximately 600 m, and the interevent distances are mostly in the range of 50–400 m (Fig. S8). Simultaneously, the source radii of the 38 events are on the order of 100 m, indicating a partial source overlap between the events (Fig. 3). Still, due to the limited resolution of our observational system, we cannot exclude the possibility that events originate on very closely spaced subparallel fault branches (as described in Shearer *et al.*, 2024). Hence, we cannot conclude true anti-repeaters (Cesca *et al.*, 2024). In effect, we also observe a weak upward migration over time. In particular, between 2015 and 2024, the observed rise in hypocenters seems to be about 100–200 m. Given the restricted network geometry, depth resolution is also limited, but the *S*–*P* travel-time figures in Figures S2–S4 strongly corroborate the indicated variation of hypocenters with time, the same as the incrementally decreased waveform similarity between earlier and later events shown in Figure S11.

Based on equation (1), we compute the slip of the individual events of the series by assuming $\mu = 60$ GPa. Figure 3c discloses some interesting observations:

1. Compared with the average recurrence time of the sequence (*tr* = 175 d), three out of five retrograde events occur shortly after a prograde event (*tr* = 26 d, see Fig. S8). When the cc threshold is slightly lowered to abs (cc) > 0.90, this is also true for the two remaining reverse events, with id numbers 1 and 6 in Figure 3 (compare with Fig. S14).
2. The reverse-polarity events are generally of small magnitude and small slip. In particular, they are always smaller in magnitude than their prograde predecessors.
3. Although prograde events have been monitored during the complete recording period from 2007 to 2024, no reverse event has occurred after the end of 2017.

The decay of observed reverse-polarity event-activity with time becomes more evident when we relax the cc threshold to cc ≤ −0.90 instead of cc ≤ −0.95. This increases the number of detected events from 38 to 131 (Fig. S14), and the activity of the entire structure is split into two phases. From 2007 to 2014, the number of prograde and retrograde events is comparable (30↔30). From 2014 onward, only three more reverse events are observed (3↔68).

We also intended to determine the source mechanisms of series cID120, but unfortunately no stable solutions could be produced. A detailed description of our approach is provided in the supplement. The predominant reason for the instability in our inversion attempts is the small event magnitudes (<3.5), combined with their great depths (>100 km), the large azimuthal gap of the station distribution (compare with Fig. 2), and the complex velocity structure of the subduction zone. As a consequence, we miss direct information on in situ stress conditions, limiting the interpretability of our observations.

Discussion

Only four out of 3153 repeater families in North Chile contain one or more events with highly anticorrelated waveforms, which affirms the peculiarity of the phenomenon.

The observed reverse-polarity event families are located at intermediate depth, different from the majority of regular repeating earthquake sequences, which are located at shallower depth along the plate interface and are usually explained by brittle failure of asperities embedded in a creeping environment (Nadeau and McEvilly, 1999; Igarashi *et al.*, 2003).

From the presented evidence, we still cannot answer with confidence whether the reverse-polarity sequence cID120 is a true or a quasi-anti-repeater group (compare with Cesca *et al.*, 2024). Our preferred interpretation is that the group is active on or along the same small-scale structure, undergoes similar stress changes, and earthquake interaction appears likely, but source overlap is not definitely established.

Two widely accepted physical mechanisms responsible for intermediate-depth seismicity are thermal runaway (e.g., John *et al.*, 2009) and dehydration embrittlement (Peacock, 2001). Thermal runaway depends on shear heating and requires relatively dry environments. In contrast, dehydration embrittlement, where nucleation is largely driven by mineral phase change reactions, involves fluid release and volumetric changes (Ferrand *et al.*, 2017). An increased Gutenberg–Richter *b* value has been observed in several subduction zones, for example, Alaska, New Zealand, and Japan (Kita and Ferrand, 2018) and is commonly interpreted as an indication of fluid abundance, which supports the possibility of dehydration embrittlement. Also for North Chile, where the rate of intermediate-depth seismicity is unusually high (Sippl *et al.*, 2019), a strongly increased *b* value has been found at the top of the intermediate-depth cloud and along the projected plate interface (Folesky, 2024). Attenuation tomography shows a pronounced low-*Q* anomaly in the overlying mantle wedge, which is also attributed to migrating fluids released from the oceanic slab (Schurr *et al.*, 2003).

Although we were not able to resolve the source mechanisms of series cID120, moment tensor solutions for larger earthquakes in the region of the 133-km-deep series show a dominance of normal-faulting mechanisms, including volumetric components (Bloch *et al.*, 2018; Sippl *et al.*, 2019). These can be explained by the slab pull regime acting in this depth range (Sippl *et al.*, 2023), possibly reactivating former outer rise bend faults that rotated over time (Malatesta *et al.*, 2024). Malatesta *et al.* (2024) modeled narrow spatial fluctuations of overpressure and underpressure within the

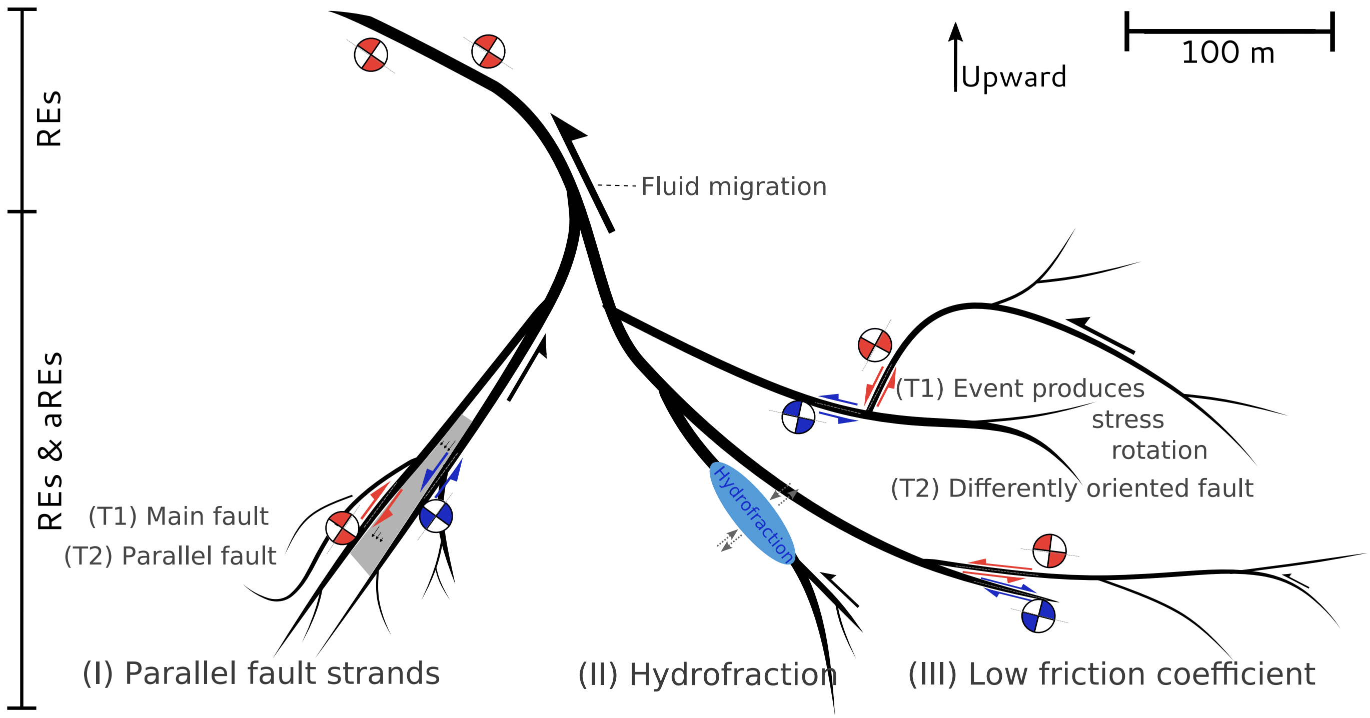

Figure 4. Tentative conceptual drawing of an intermediate-depth dewatering structure that may host prograde (red) and reversed polarity events (blue) in its earlier stage, whereas in its later, upper part only prograde events are observed. (I) Parallel fault strands bordering a sliding block that host two earthquakes at times T1 and T2 due to stress transfer. (II) Hydrofracture growth or opening. (III) Unfavorably oriented faults that host events due to an extremely low friction angle. This figure is motivated by the models proposed by Cesca *et al.* (2024) in their figure 2.

downgoing plate in regions where the plate is bent, located at reactivated faults that were formed as outer rise bend faults before subduction. In these regions of strong stress heterogeneity, the occurrence of opposed mechanisms may be possible, but presumably not at a very short scale of tens of meters, as observed in our case study.

We rather presume that the observed characteristics of the sequence, in particular the small interevent distances, short waiting times of events with reversed polarity, and weak upward migration of seismicity with time, argue for the presence of a complex fault network and high fluid pore pressure, low fault friction, small deviatoric stresses, or a combination of them.

Figure 4 depicts a conceptual framework to explain the observed intermediate-depth reversed polarity sequence, acting on models discussed by Cesca *et al.* (2024). We suggest that seismicity is proximately related to an evolving network structure. Dehydration reactions of subducted hydrous minerals (whose distribution can also be inherently heterogeneous), for example, due to earlier outer rise faulting (Malatesta *et al.*, 2024), release water, forming a branched fluid network (Huber *et al.*, 2024). The increase in fluid pore pressure and the reduction in the fault friction coefficient, together with complex fault orientations, may then explain the occurrence of earthquakes with reverse polarity by one of the three mechanisms (I)–(III) illustrated in Figure 4.

The significant increase in detected events and, in particular, the increased fraction of reverse-polarity events observed when lowering the cc threshold to cc = −0.90 (Fig. S14) also complies with the assumed structural heterogeneity. The record of reverse-polarity events ceases in 2017, whereas the series itself remains active until the end of the recording period in 2024. Together with the weak upward migration of seismicity observed after 2015, this would map a more efficient upward fluid migration path, possibly oriented optimally to the in situ stress field and favoring a consistent and uniform source mechanism in the second phase.

In the proposed model, the occurrence pattern of the reverse-polarity sequence indicates transient, dehydration- and fluid-driven processes on the timescale of years and a spatial scale of a few hundred meters. Preferentially, it occurs in a domain of inherited structural heterogeneity. This may explain partly why observations of this phenomenon seem to be so rare. Nevertheless, note here that most routine waveform-similarity-based studies to date use exclusively positive correlation values and, therefore, might miss some reversely polarized event pairs.

There are alternate explanations for quite similar observations. In particular, Nakajima *et al.* (2013) attribute a highly active seismic cluster which contains reverse mechanism events beneath Japan at 150 km depth to delayed eclogitization in the oceanic lower crust as a source of volume reduction which, in effect, may produce reversed mechanisms. The delay is attributed to grain size differences, substantially less alteration, and lower temperatures inside the oceanic plate, which results in the eclogitization progressing from the top of the crust downward. A similar observation and interpretation was reported by Plourde and Bostock (2019) for events in the Yakutat seismic cluster, Alaska, at 125 km depth.

These two studies differ from our observations at least two ways. First, they report a depth-dependent spatial separation of normal- and reverse-faulting mechanisms, whereas we observe no such separation. Second, neither study describes a temporal dependence, which is a prominent and significant feature in our data.

Compared with most previously reported cases (Cesca *et al.*, 2026), the spatial resolution of the series studied here in northern Chile is higher, revealing activity concentrated within a volume of only a few hundred meters and no spatial separation between opposite-polarity events. This close spatial proximity rules out the delayed eclogitization model here. The spatial and temporal patterns of the earthquake sequence suggest that it maps a transient fluid-related process, possibly a fluid-release structure evolving from one state to a subsequent state. Unfortunately, the source mechanisms could not be determined. We hope that the work presented here may motivate similar detailed studies in other regions of the world, which could help better resolve and explain the peculiar seismological feature of reverse-polarity earthquakes at intermediate depth.

Data and Resources

All software used in this work is open source. The repeater catalog is available at Zenodo (zenodo.org/records/16738820). The seismicity catalog is available at GeoForschungsZentrums (gfzpublic.gfz.de/pubman/item/item_5018559). Seismic data were obtained from the GEOPHONE web page available at geofon.gfz-potsdam.de/waveform/. All websites were last accessed in July 2026. The supplemental material for this article contains (1) a description of the localization method; (2) supplementary waveform figures; (3) magnitude and event parameter plots; (4) location and cross-correlation coefficient (cc)-matrix plots; (5) slip history for a decreased cc = 0.90; and (6) a description of the moment tensor inversion attempt.

Declaration of Competing Interests

The authors acknowledge that there are no conflicts of interest recorded.

Acknowledgments

J. F. was funded by the German Science Foundation (DFG), Project Numbers FO 1325/3-1. The authors thank the editor, Vera Schulte-Pelkum, and two anonymous reviewers for constructive comments. The authors also thank Peter Niemz and Simone Cesca for sharing their concept model drawings and for discussions that motivated this work.

References

Bloch, W., B. Schurr, J. Kummerow, P. Salazar, and S. A. Shapiro (2018). From slab coupling to slab pull: Stress segmentation in the subducting Nazca plate, *Geophys. Res. Lett.* **45,** no. 11, 5407–5416.

Buitinck, L., G. Louppe, M. Blondel, F. Pedregosa, A. Mueller, O. Grisel, V. Niculae, P. Prettenhofer, A. Gramfort, J. Grobler, *et al.* (2013). API design for machine learning software: Experiences from the Scikit-learn project, *ECML PKDD Workshop: Languages for Data Mining and Machine Learning*, 108–122.

Cesca, S., P. Niemz, T. Dahm, and S. Ide (2024). Anti-repeating earthquakes and how to explain them, *Commun. Earth Environ.* **5,** no. 1, 158.

Cesca, S., D. Stich, G. Ekström, P. Niemz, R. Moya Sánchez, S. Ide, and T. Dahm (2026). Opposite faulting in global seismicity, *The Seism. Rec.* **6,** no. 1, 85–95.

Eshelby, J. D. (1957). The determination of the elastic field of an ellipsoidal inclusion, and related problems, *Proc. Math. Phys. Sci.* **241,** 376–396.

Ferrand, T. P., N. Hilairet, S. Incel, D. Deldicque, L. Labrousse, J. Gasc, J. Renner, Y. Wang, H. W. Green Ii, and A. Schubnel (2017). Dehydration-driven stress transfer triggers intermediate-depth earthquakes, *Nat. Commun.* **8,** no. 1, 15,247.

Folesky, J. (2024). Different earthquake nucleation conditions revealed by stress drop and b-value mapping in the northern Chilean subduction zone, *Sci. Rep.* **14,** no. 1, 12,182.

Folesky, J., J. Kummerow, and L. J. Hofman (2025). A repeating earthquake catalog for northern Chile, *Seismica* **4,** no. 2, doi: 10.26443/seismica.v4i2.1578.

Folesky, J., C. Pennington, J. Kummerow, and L. Hofman (2024). A comprehensive stress drop map from trench to depth in the northern Chilean subduction zone, *J. Geophys. Res. Solid Earth* **129,** no. 1, e2023JB027549, doi: 10.1029/2023JB027549.

Hanks, T. C., and H. Kanamori (1979). A moment magnitude scale, *J. Geophys. Res. Solid Earth* **84,** no. B5, 2348–2350.

Huber, K., T. John, J. C. Vrijmoed, J. Pleuger, and X. Zhong (2024). Pulsed fluid release from subducting slabs caused by a scale-invariant dehydration process, *Earth Planet. Sci. Lett.* **644,** 118924.

Igarashi, T., T. Matsuzawa, and A. Hasegawa (2003). Repeating earthquakes and interplate aseismic slip in the northeastern Japan subduction zone, *J. Geophys. Res. Solid Earth* **108,** no. B5, doi: 10.1029/2002JB001920.

Integrated Plate boundary Observatory Chile (IPOC) (2006). IPOC Seismic Network. Integrated Plate boundary Observatory Chile - IPOC, *GFZ German Research Centre for Geosciences; Institut des Sciences de l'Univers-Centre National de la Recherche CNRS-INSU, Seismic Network*, doi: 10.14470/PK615318.

John, T., S. Medvedev, L. H. Rüpke, T. B. Andersen, and H. Austrheim (2009). Generation of intermediate-depth earthquakes by self-localizing thermal runaway, *Nature Geosci.* **2,** 137–140.

Kita, S., and T. P. Ferrand (2018). Physical mechanisms of oceanic mantle earthquakes: Comparison of natural and experimental events, *Sci. Rep.* **8,** no. 1, 17049.

Lomax, A., J. Virieux, P. Volant, and C. Berge-Thierry (2000). Probabilistic earthquake location in 3D and layered models, in *Advances in Seismic Event Location*, C. H. Thurber and N. Rabinowitz (Editors), Vol. 18, Springer, Netherlands, 101–134, doi: 10.1007/978-94-015-9536-0_5.

Lu, W., S. Ide, and H. Yue (2025). Small-scale stress heterogeneity inferred many anti-repeating earthquakes in sierra valley, Nevada, *Earth Planets Space* **77,** no. 1, 142.

Ma, X., and Z. Wu (2013). 'Negative repeating doublets' in an aftershock sequence, *Earth Planets Space* **65,** no. 8, 923–927.

Malatesta, C., T. Gerya, S. Pittaluga, and D. Cabiddu (2024). Intermediate-depth seismicity and intraslab stress changes due to outer-rise faulting, *Commun. Earth Environ.* **5,** no. 1, 253.

Nadeau, R. M., and T. V. McEvilly (1999). Fault slip rates at depth from recurrence intervals of repeating microearthquakes, *Science* **285,** no. 5428, 718–721.

Nakajima, J., N. Uchida, T. Shiina, A. Hasegawa, B. R. Hacker, and S. H. Kirby (2013). Intermediate-depth earthquakes facilitated by eclogitization-related stresses, *Geology* **41,** no. 6, 659–662.

Peacock, S. M. (2001). Are the lower planes of double seismic zones caused by serpentine dehydration in subducting oceanic mantle? *Geology* **29,** no. 4, 299–302.

Plourde, A. P., and M. G. Bostock (2019). Relative moment tensors and deep Yakutat seismicity, *Geophys. J. Int.* **219,** no. 2, 1447–1462.

Prieto, G. A., G. C. Beroza, S. A. Barrett, G. A. López, and M. Florez (2012). Earthquake nests as natural laboratories for the study of intermediate-depth earthquake mechanics, *Tectonophysics* **570,** 42–56.

Schurr, B., G. Asch, A. Rietbrock, R. Trumbull, and C. Haberland (2003). Complex patterns of fluid and melt transport in the central Andean subduction zone revealed by attenuation tomography, *Earth Planet. Sci. Lett.* **215,** no. 1, 105–119.

Shearer, P. M., N. Shabikay Senobari, and Y. Fialko (2024). Implications of a reverse polarity earthquake pair on fault friction and stress heterogeneity near Ridgecrest, California, *J. Geophys. Res. Solid Earth* **129,** no. 11, e2024JB029562, doi: 10.1029/2024JB029562.

Sippl, C., B. Schurr, T. John, and S. Hainzl (2019). Filling the gap in a double seismic zone: Intraslab seismicity in northern Chile, *Lithos* **346,** 105155.

Sippl, C., B. Schurr, J. Münchmeyer, S. Barrientos, and O. Oncken (2023). The Northern Chile forearc constrained by 15 years of permanent seismic monitoring, *J. South Am. Earth Sci.* 104326, doi: 10.1016/j.jsames.2023.104326.

Trugman, D. T., Z. E. Ross, and P. A. Johnson (2020). Imaging stress and faulting complexity through earthquake waveform similarity, *Geophys. Res. Lett.* **47,** no. 1, e2019GL085888, doi: 10.1029/2019GL085888.

Uchida, N., and R. Bürgmann (2019). Repeating earthquakes, *Annu. Rev. Earth Planet. Sci.* **47,** 305–332.

Manuscript received 16 April 2026
Published online 28 July 2026